CONFERENCE PRE-PRINT

EDGE MAGNETIC ISLANDS AND ITS APPLICATION TO THE DEVELOPMENT OF ADVANCED DIVERTOR CONFIGURATION ON THE J-TEXT TOKAMAK

¹Y. LIANG, ²S. ZHOU, ³J. YANG, ^{1,2}J.K. HUA, ¹Y.T. YANG, ²W. XIE, ²N.C. WANG, ⁴X.L. ZHANG, ¹A. KNIEPS, ¹S. XU, ¹E.H. WANG, ²Z.P. CHEN, ²B. RAO, ²Z.F. CHENG, ²Q.H. YANG, ²W. YAN, ²Z.Y. CHEN, ²Y.H. DING, ⁵Y. SUZUKI, ¹C. LINSMEIER, AND THE J-TEXT TEAM

Email: y.liang@fz-juelich.de

Abstract

A preliminary exploration of island divertor formation using resonant magnetic perturbation (RMP) coils was conducted on J-TEXT, revealing a self-sustained divertor oscillation linked to edge magnetic island dynamics. This bifurcative oscillation (~50 Hz), involving periodic transitions in edge island width, Hα intensity, and electron temperature, reflects repeated magnetic field penetration and screening, gradually diminishing as the divertor target intersects the islands. The oscillation's behavior shifts from burst-like to quasi-continuous, influenced by the divertor structure and plasma edge density, though detailed mechanisms require further study. Additionally, experiments showed that RMP-induced m/n=3/1 magnetic islands can enhance impurity screening, especially when the island's O-point is near the low-field side limiter, affecting impurity behavior. The study also found that the heat flux distribution on the divertor target varies significantly with the edge magnetic topology. Moreover, hydrogen fueling via supersonic molecular beam injection (SMBI) can induce power detachment, as radiation fronts approach the last closed flux surface after SMBI pulses, offering a promising method to achieve divertor detachment in devices with complex 3D magnetic structures.

1. INTRODUCTION

The development of advanced magnetic divertor configurations to solve the core-edge integration, the coupling of heat and particle exhaust and impurity control in high-power high-performance long-pulse plasma operation is one of the important topics in current fusion research, and is being carried out in more and more tokamak and stellarator devices. The island divertor, one of multiple attractive advanced divertor concepts, has been successfully applied on the W7-AS stellarator, and further developed on the W7-X stellarator. In the island divertor configuration, the SOL is formed by a group of magnetic islands, which form closed flux tubes around the core plasma. These edge islands are then intersected and cut open by divertor target plates. Compared with the standard poloidal divertor configuration, the island divertor configuration has a weaker correlation with the plasma current and a longer connection length, which results in a wider distribution of heat loads and also makes it easier to enter stable detachment of divertor operation [1]. Therefore, it is of great interest and significance to apply and explore the island divertor configuration in tokamak plasmas. Recently, a first attempt has been made to form an island divertor configuration in the J-TEXT tokamak [2, 3].

¹ Forschungszentrum Jülich GmbH, Institute of Fusion Energy and Nuclear Waste Management – Plasma Physics, 52425 Jülich, Germany

² Huazhong University of Science and Technology, Wuhan 430074, China

³ Institute of Metal Research Chinese Academy of Sciences, Shenyang, China

⁴ Southwestern Institute of Physics, Chengdu 610041, People's Republic of China

⁵ Hiroshima University, Higashi-Hiroshima, Japan

2. RMP COILS ON J-TEXT

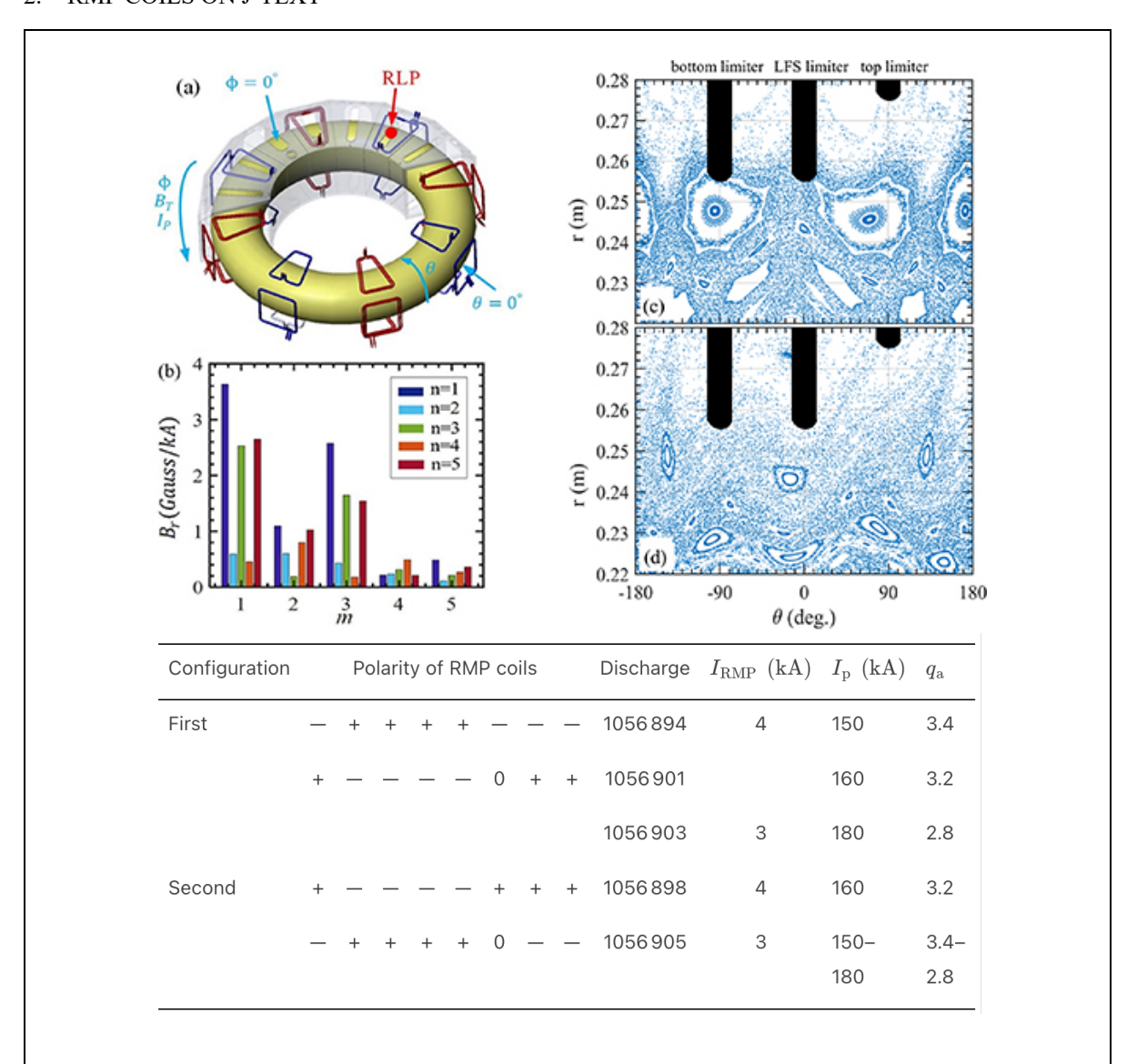


Figure 1. (a) Layout of the RMP coils in J-TEXT, and the position of the reciprocating Langmuir probe. (b) 2D Fourier (m, n) spectrum of the radial magnetic field generated by RMP coils at the plasma edge. (c)–(d) Poincaré plots of the plasma cross-section ϕ_{tol} = 337.5° for first and second RMP configurations, with three limiters at ϕ_{tol} = 337.5° indicated by black rectangles. The real parameter settings used in the prediction of magnetic topology are from discharges 1056901 and 1056898. Lower table shows the RMP coil setup and plasma parameters implemented in the experiment. [3]

J-TEXT is a conventional medium-sized tokamak with a major radius of $R_0 = 1.05$ m and minor radius of a = 0.25-0.29 m [5]. There are four titanium-carbide-coated graphite rail limiters, one of which is fixed at the high field side (HFS) with a toroidal angle of $\phi_{tor} = 247.5^{\circ}$, a width of 0.058 m in the toroidal direction and a minor radii of 0.265 m from the center of the vacuum chamber; and the other three are movable and located in different poloidal positions (top, middle at the low field side (LFS) and bottom) at $\phi_{tor} = 337.5^{\circ}$ with a width of 0.050 m in the toroidal direction. In this experiment, these three movable limiters are placed at the minor radii of 0.275 m, 0.255 m, and 0.255 m, respectively. The parameters in Ohmic hydrogen discharge for this experiment are: plasma current $I_p = 150 - 180 \, kA$, toroidal magnetic field $B_t = 1.4 \, T$, the central line-averaged electron density $n_e = (1.2 - 1.4) \times 10^{19} \, m^{-3}$ and the edge safety factor is $q_a = 2.7 - 3.4$.

As shown in figure 1 (a), two sets of in-vessel RMP systems are constructed along the torus, consisting of 24 saddle coils situated at 8 toroidal locations and 3 poloidal locations (top, middle at LFS and bottom) [6]. The red coil set is the double-turn type, while the blue coil set is the single-turn type. In this experiment, the top and bottom coils are employed to produce a static RMP with a large m/n=3/1 resonant component. The spectrum of the RMPs, calculated without taking plasma responses into account (in vacuum conditions), is depicted in figure 1 (b), where the m/n=3/1 component at the plasma edge is $B_r^{3/1}=2.58~Gs/kA~(\sim 7.4\times 10^{-4}~\text{of}~B_t~\text{in}$ the case of RMP current $I_{RMP} = 4 kA$). Two RMP configurations are performed by altering the polarity of the RMP coil current, as summarized in the second column of the Table 1, where the symbol '+ (-)' denotes an outward- (inward-) pointing B_r . The corresponding Poincaré plots, calculated with $I_p = 160 \, kA \, (q_a = 3.2)$ by the 3D non-linear magnetohydrodynamical (MHD) equilibrium code HINT [7], of the plasma cross-section $\phi_{tor} = 337.5^{\circ}$ are shown in figure 1 (c) and (d). In the first RMP configuration, the O-point of m/n=3/1 magnetic island faces the bottom limiter. While in the second RMP configuration, the O-point faces the LFS limiter with a poloidal shift towards the bottom side. Due to the different poloidal positions of magnetic islands, different intersection patterns occur between the edge magnetic islands and the poloidally localized limiters for the two configurations when the island is pushed outward. Furthermore, for the second RMP configuration, the stochastization around the boundary island is enhanced, which is due to the high-order modes generated by the missing coil at the bottom side of port 10.

3. FORMATION OF ISLAND DIVERTOR CONFIGURATION

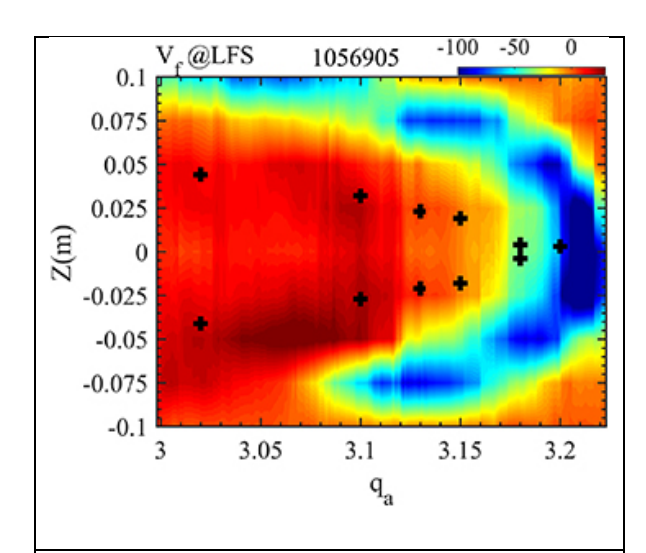


Figure 2. Dependence of LFS floating potential distribution on edge safety factor q_a . The black crosses are the strike points obtained from the field lines with the deepest penetration into the core plasma calculated by the field line tracing. [3]

J-TEXT, the first island configuration was formed by moving the m/n = 3/1edge island chain outward to intersect with the divertor target. Here, m and n are the poloidal and toroidal mode numbers, respectively. In this experiment, the m/n = 3/1edge magnetic islands were excited by applying RMPs with a dominant m/n = 3/1 component [4] in a limiter plasma with an edge safety factor, qa, slightly over 3. By increasing the plasma current to reduce the edge safety factor, the edge magnetic islands are cut by the divertor target to finally build up the island divertor configuration. When the 3/1 edge islands are gradually opened by the divertor target, the main striking points, indicated by the floating potential measurements from the divertor Langmuir probe arrays, move to two sides of the divertor target as shown in figure 2. This reveals that topological differences considerably affect the divertor heat load patterns. Once the 3/1 edge islands are fully moved behind the divertor target, the island divertor configuration is then transformed back to a limiter configuration.

The formation of the island divertor configuration strongly depends on the edge magnetic topologies, or more specifically, the interactions between the edge island and the divertor target. By optimizing the edge magnetic topology and the structure of the target plate, the divertor heat load distribution could be significantly modified, so as to increase the power deposition area and reduce the peak heat load. Such optimization processes are being carried out on J-TEXT, leveraging both 3D edge transport modelling and dedicated experiments.

4. STABILITY OF EDGE ISLAND

The operation of the island divertor configuration is closely tied to the stability of the edge island. Once there is a change in the width and phase of the edge island, the island divertor configuration cannot operate stably, which can even lead to the deposition of heat load outside the divertor targets. Therefore, the stability of the edge island is of great concern in the experiment [8].

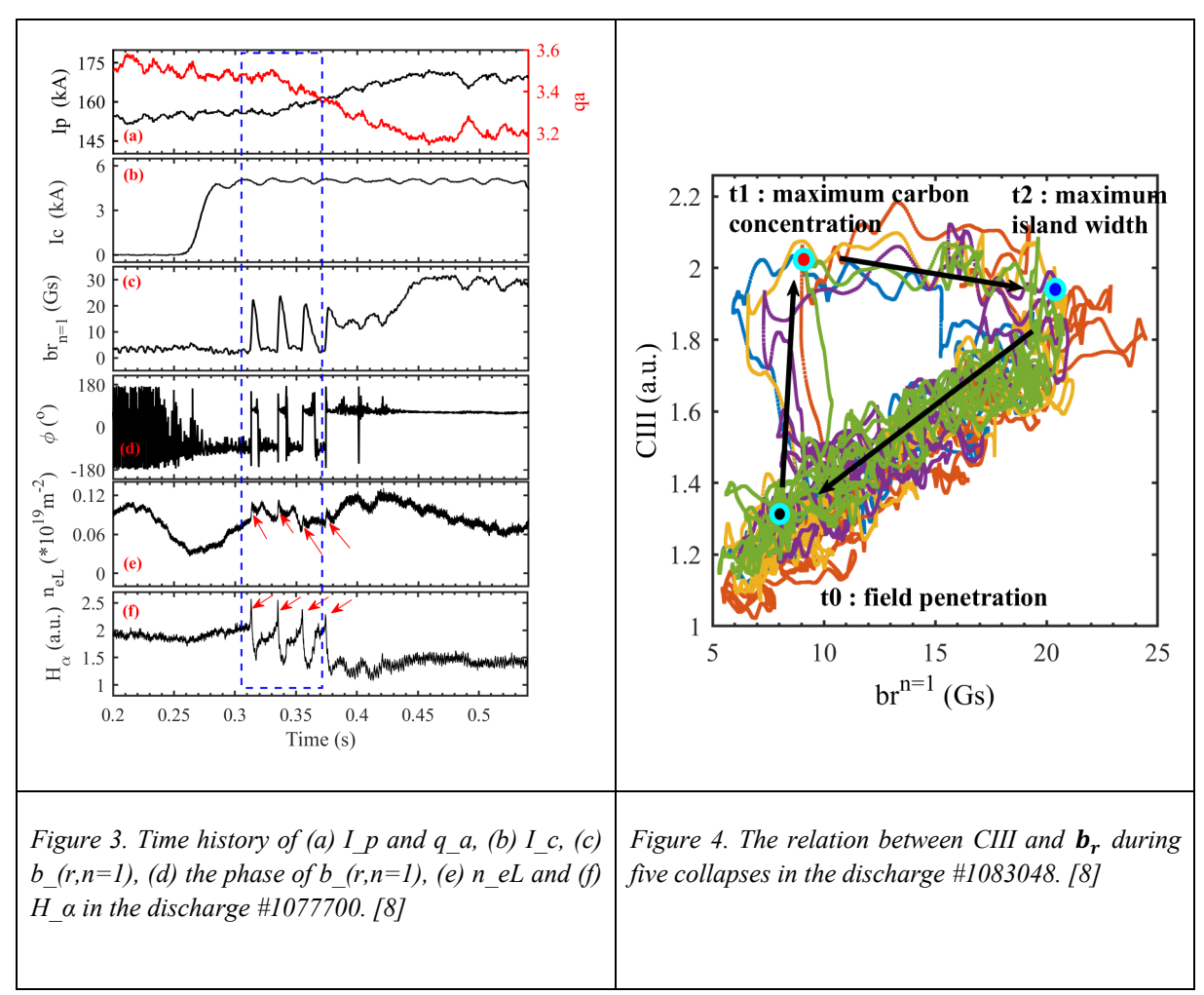


Figure 3 shows time evolution of the plasma toroidal current, I_p , and q_a , the RMP coil current, I_c , the amplitude and the phase of $b_{(r,n=1)}$, central line integrated electron density, n_eL and intensity of H_a emission measured in the discharge #1077700 on J-TEXT. A scan of q_a is conducted by increasing I_p while keeping $B_T = 1.7 \, T$. The I_c ramps up to 4 kA from $t = 0.26 \, s$ to $t = 0.28 \, s$, and it is maintained for the whole discharge. Three instances of field penetration and collapse occur between $t = 0.303 \, s$ and $t = 0.375 \, s$ (q_a decreases from 3.46 to 3.35). This is indicated by a blue dotted line box in Figure 2. In this process, the q=3 resonant surface moves outward as q_a decreases. On one hand, this enhances the amplitude of the $m/n = 3/1 \, RMP$ at the resonant surface. On the other hand, it leads to the $m/n = 3/1 \, RMP$ are the resonant in the sum of th

The final field penetration and collapse occur at t=0.374 s, and the m/n=3/1 magnetic island no longer disappears afterward. The width of the m/n=3/1 magnetic island begins to grow as q_a decreases after t=0.39 s, and remains nearly constant when q_a keeps unchanged, as shown in figure 3 (c) and (d). Figure 3 (e) and (f) present the evolution of electron density and particle recycling. During periodic collapse, burst-like behaviors are observed in both signals. When the m/n=3/1 magnetic island is located stably at the plasma boundary after t=0.39 s, the particle recycling remains almost unchanged. The density slowly decreases as decreasing q_a , which may be attributed to a pump-out effect. In summary, the periodic collapse phenomenon disappears at q_a above 3.35. A stable island divertor configuration is established.

Figure 4 shows the relationship between the boundary CIII signal and the $b_{r,n=1}$ signal during four collapses in the discharge #1083048. Obviously, after the field penetration, carbon impurities rapidly enter the plasma boundary and reach their maximum concentration ($t_0 \sim t_1$), despite the magnetic island width remaining small. Subsequently, as the magnetic island continues to grow to its maximum width, the carbon impurity concentration changes insignificantly ($t_1 \sim t_2$). Eventually, the magnetic island cannot be sustained and gradually decays, and a corresponding decline in carbon impurity concentration can also be observed ($t_2 \sim t_0$). This suggests that radiative cooling effect is one possible reason to destabilize the edge m/n = 3/1 magnetic island by the accumulation of carbon impurities. Finally, this trigger fast transport near X-point of island.

5. IMPURITY SCREENING EFFECTS

The impurity accumulation at the central plasma is one of the burning issues for high-performance long-pulse plasma operation. Impurity control has become the focus of extensive attention in J-TEXT. During the application of the island divertor configuration, it was found that the m/n = 3/1 edge island has an impurity screening effect, especially when the O-point of the island is near the LFS divertor target. By combining a methane injection experimental study and STRAHL impurity transport analysis, it was demonstrated that the variation of the impurity transport dominates the impurity screening effect. The impurity diffusion is enhanced with a significant increase in the outward convection velocity at the edge region [9]. The interactions of the edge island and the divertor target contribute to the impurity screening effects with the dependence on the edge island width and phase. Therefore, a better impurity exhaust/screening could also be achieved by optimizing the edge magnetic topologies.

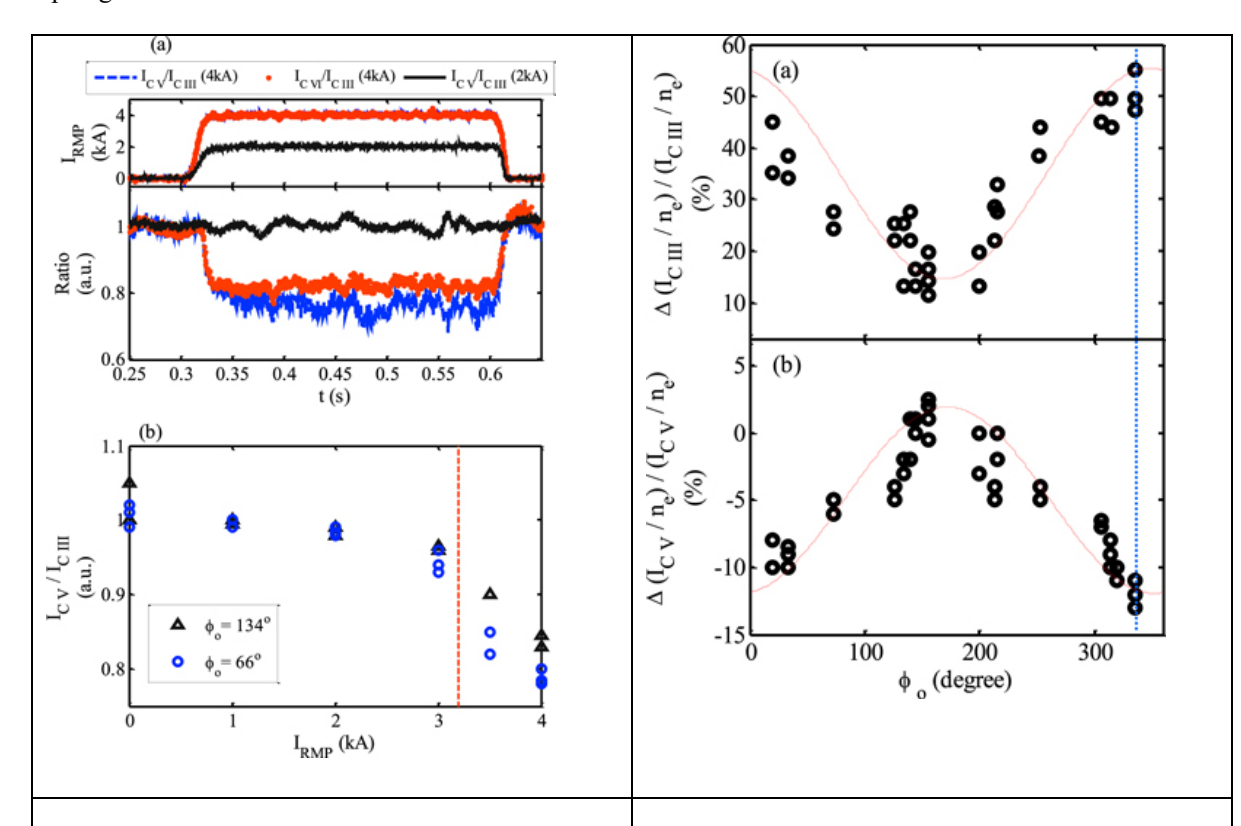


Figure 5. (a) Current of RMP; evolution of the ratio of I_C v/I_C III (blue dotted line) and I_C v/I_C III (red dots) with IRMP = 4 kA, I_C v/I_C III (black line) with I_{RMP} = 2 kA. (b) Statistical relationship between ratio of I_C v/I_C III and RMP current; red dashed line indicates the threshold of 3/1 penetration.[9]

Figure 6. Normalized statistical results of RMP phase (ϕ_o) and relative variation of the $I_{C\ V}/n_e$ and $I_{C\ III}/n_e$ with 3/1 locked magnetic island induced by the RMP penetration. The blue dotted line indicates the LFS limiter position.[9]

In this experiment, the emission intensity ratio of the inner impurity (C V or C VI) and the outer impurity (C III) is used to reflect the carbon screening effect, as shown in figure 4. Since the 3D edge magnetic topology leads to an asymmetric C III distribution, the C III signal is deduced by averaging the C III signals from multiple places. It is found that the impurity screening effect increases with an increase in RMP current, showing a decline in the ratio $I_{\text{C V}}/I_{\text{C III}}$. The effect appears much more sensitive on the RMP penetration, with $I_{\text{RMP}} \ge 3.2$ kA, corresponding to the further significant drop after the red dashed line in figure 4(b). The RMP phase is found to impact the impurity screening effect as well, showing that the normalized ratio of $I_{\text{C V}}/I_{\text{C III}}$ in the case with $\phi_0 = 134^\circ$ RMP penetration is higher than that with $\phi_0 = 66^\circ$.

Figure 6 presents the relative variation of C V and C III emission with the scanned RMP phases, where the plasma parameters are fixed as $I_P = 170$ kA, $B_T = 1.7$ T, and $n_e = (1.2-1.5) \times 10^{19}/\text{m}^3$. The field penetrations are induced using the same RMP strength with a coil current of 4 kA. The dependence of the carbon emission on the RMP phase can be well described by $\Delta I/n_e = b + k\sin(\phi_0 + \alpha)$ for both C V and C III, where k, a, and b are constants. However, the ϕ_0 dependence is opposite for the two impurity ions, i.e. $\alpha_{\text{C III}} - \alpha_{\text{C V}} \sim 180^{\circ}$. This clearly shows the dependence of the carbon emission on the RMP phase, where the evolutions of C V and C III variation both follow the cosine function, but in the opposite phases. The cycle length is 360°, in line with the toroidal mode number (n = 1) of the RMP field.

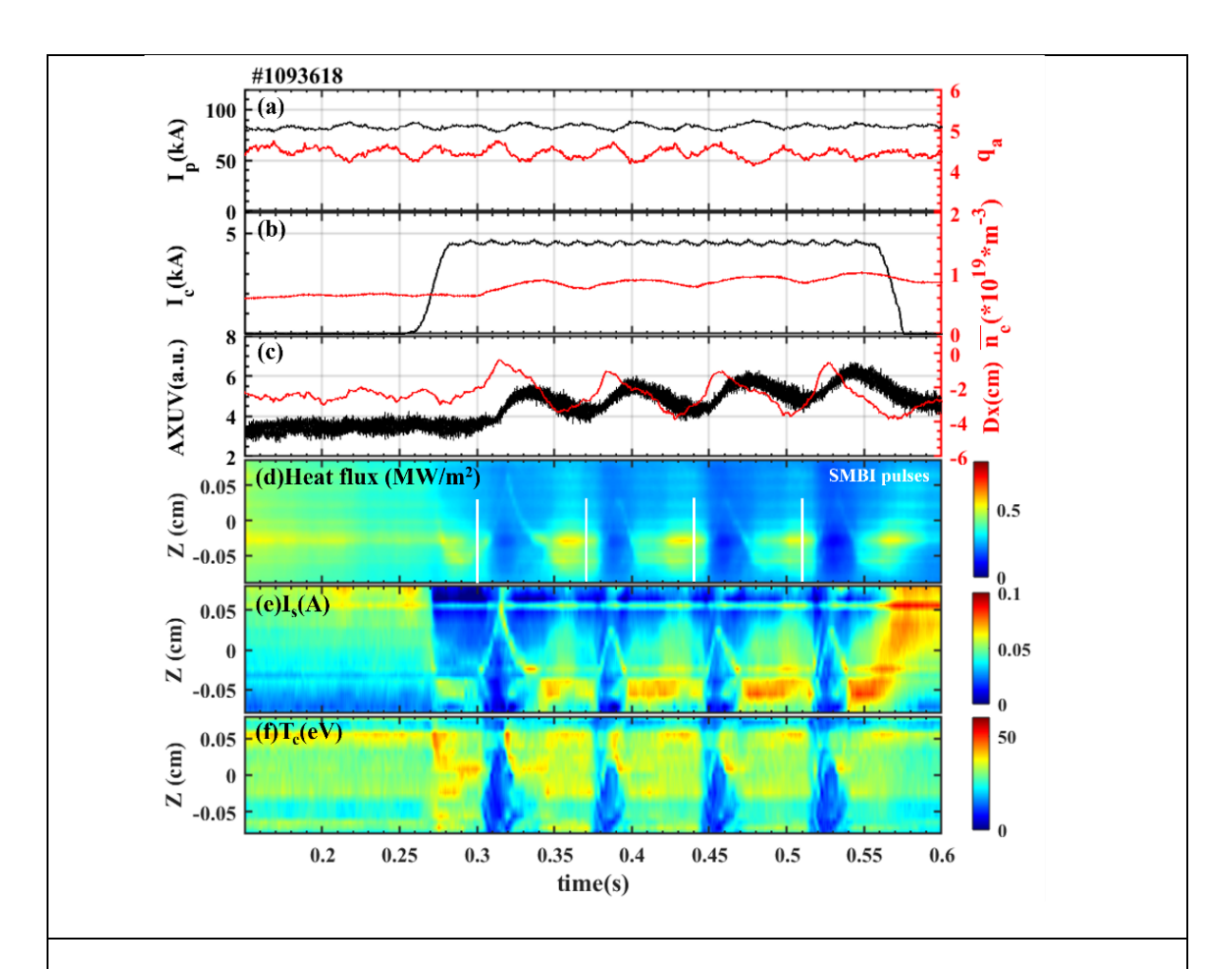


Figure 7. #1093618 Time evolution of (a) I_P and q_a , (b) the I_c and central line-averaged density \overline{n}_e , (c) the total radiation loss and the horizontal displacement of plasma, (d) the HFS target heat flux distribution and the SMBI injection time, (e) the contour of the ion saturation current I_s , (f) the contour of the electron temperature T_e . [11]

In addition, the radial electric field, the plasma rotation, and turbulence are considered to play an important role in impurity screening. The detailed impurity behaviors under the island divertor configuration will be studied with the foreseen application of 3D transport codes, such as EMC3-EIRENE. Moreover, combining the electric field, plasma rotation, and turbulence into integrated scenario modeling is another important topic for further studies.

6. 3D DIVERTOR HEAT LOADS

For the island divertor configuration, longer field-line connection lengths at the SOL (in the magnitude of 102–103 m, much longer than the electron mean free path) could be obtained, which benefits heat load spreading on the divertor target [10]. In order to investigate the effects of the edge magnetic topology on the divertor heat load distribution, a 2D infrared thermography camera system viewing the HFS divertor target from the LFS midplane window with a high spectral resolution of 0.5 mm was established on J-TEXT. During the experiments in island divertor configuration, the surface temperature distributions on the divertor target could be obtained in real time.

Figure 7 shows the time evolution of plasma parameters of discharge #1093618, which is one pure Ohmic discharge with multi-pulses of SMBI on J-TEXT. In this discharge, $B_T = 1.6T$ and $I_P = 80kA$, which corresponds to $q_a \sim 4.3$. The central line-averaged density $\overline{n_e}$ was maintained around $0.6 \times 10^{19} m^{-3}$ before SMBI pulses. The island divertor coils current was applied at t = 0.25s, and the I_c ramped up to maximum value (-4.5kA) at t = 0.27s. The m/n = 4/1 magnetic island occurred at the boundary of plasma and was opened by the HFS target plate, which leads to the sudden change of the heat flux pattern (Figure 7 (d)) and the ion saturation current I_s (Figure 7 (e)). Four SMBI pulses of hydrogen gas were injected into the plasma with the same backing pressure of 0.18MPa and each pulse width is 2ms, corresponding to an estimated number of molecules of approximately 0.61×10^{19} per pulse. The experimental results show that the heat flux on the HFS target plate experiences a significant reduction in delay following each SMBI injection. The precise delay time cannot be determined due to constraints in the time resolution of the IR camera. Meanwhile, there will be a movement of the strike-points on the target plate due to horizontal displacement as shown in figure 7 (d). The total radiated power measured by AXUV arrays (Figure 7 (c)), started to rise after each SMBI pulse and then decreased after reaching saturation. The peak heat flux reduced significantly in the process of AXUV increase and then slowly returned to the initial level before the next SMBI pulse. As shown in figure 7 (e) and (f), although the ion saturation current and electron temperature decreased to some extent after SMBI pulses, they did not decrease to the threshold of detachment. It should be noted that the experiment did not achieve particledetachment, but the power-detachment was realized by SMBI gas fuelling [11].

The key points of the island divertor research on J-TEXT are to demonstrate its performances of heat and particle exhaust. Moreover, it is worthwhile to explore how to realize stable detachment operation of the island divertor, which may rely on the synergy effects of the optimized magnetic topology, plasma transport, and heat load dissipation. In particular, the core—edge integration to develop and demonstrate dissipative/detached divertor solutions for power and particle control, sufficient for extrapolation to high-performance long-pulse H-mode plasma conditions, is worth investigating.

7. SUMMARY

A first attempt has been made to form an island divertor configuration using a set of RMP coils in the J-TEXT tokamak. A new type of edge island instability, the so-called self-sustained divertor oscillation, was observed in J-TEXT during divertor experiments. Since a bifurcative oscillation of \sim 50 Hz is observed among the edge island width, the edge H α intensity, and the edge electron temperature, the oscillation is regarded to be a sequential repetition of the magnetic field penetration-screening transition and back-transition. The periodic

collapses repeat several times until the edge islands are intersected by the divertor target. As the edge islands are gradually opened, the amplitude of the oscillation decreases, and the properties of the oscillation also change from burst-like to quasi-continuous. Thus, the divertor target structure is also significant for the stability of the edge island. In addition, the divertor oscillation shows a correlated dependence on the plasma edge density. The detailed analyses and explanations are still to be investigated.

The effect of externally applied resonant magnetic perturbation (RMP) on carbon impurity behavior is investigated in the J-TEXT tokamak. It is found that the m/n = 3/1 islands have an impurity screening effect, which becomes obvious while the edge magnetic island is generated via RMP field penetration. The impurity screening effect shows a dependence on the RMP phase with the field penetration, which is strongest if the O point of the magnetic island is near the low-field-side (LFS) limiter plate.

On J-TEXT, the experimental results show that the heat flux distribution on the HFS target plate depends significantly on the edge magnetic topology. Furthermore, the impact of hydrogen fueling using supersonic molecular beam injection (SMBI) on the divertor heat flux distributions is studied with an island divertor configuration. It has been observed that power detachment can be achieved when the radiation front approaches the last closed flux surface after each SMBI pulse. This result may provide a method of access for divertor detachment on a fusion device with a 3D boundary magnetic structure.

ACKNOWLEDGEMENTS

This work has been carried out within the framework of the EUROfusion Consortium, funded by the European Union via the Euratom Research and Training Programme (Grant Agreement No 101052200 — EUROfusion). Views and opinions expressed are however those of the author(s) only and do not necessarily reflect those of the European Union or the European Commission. Neither the European Union nor the European Commission can be held responsible for them.

REFERENCES

- [1] M. Jakubowski et al 2021 Nucl. Fusion 61 106003
- [2] Y. Liang et al 2022 Plasma Sci. Technol. 24 124021
- [3] S. Zhou, et al 2025 Nucl. Fusion 65 016020
- [4] J. Yang, et al 2024 Nucl. Fusion **64** 056030
- [5] Y. Liang, et al 2019 Nucl. Fusion 59 112016
- [6] B. Rao, et al 2014 Fusion Eng. Des. 89 378
- [7] Y. Suzuki, 2017 Plasma Phys. Control. Fusion **59** 054008
- [8] J.K. Hua, Y. Liang et al., 2025 submitted to Nuclear Fusion
- [9] X.L. Zhang et al 2021 Plasma Sci. Technol. 23 125101
- [10] S. Zhou et al 2022 Nucl. Fusion 62 106002
- [11] Y.T. Yang et al 2024 Plasma Sci. Technol. 26 125102